Solid State Nuclear Magnetic Resonance 71 (2015) 11–18

Contents lists available at ScienceDirect

Solid State Nuclear Magnetic Resonance

journal homepage: www.elsevier.com/locate/ssnmr

# DQ-DRENAR with back-to-back (BABA) excitation: Measuring homonuclear dipole–dipole interactions in multiple spin-1/2 systems

Jinjun Ren [a,*], Hellmut Eckert [b,c,*]

[a] Key Laboratory of Materials for High-Power Laser, Shanghai Institute of Optics and Fine Mechanics, Chinese Academy of Sciences, Shanghai 201800, China
[b] Institut für Physikalische Chemie, Westfälische Wilhelms-Universität Münster, Corrensstr. 30, D-48149 Münster, Germany
[c] Instituto de Física de São Carlos, Universidade de São Paulo (USP), C.P. 369, CEP 13560-970, São Carlos, SP, Brazil

ARTICLE INFO

Available online 14 October 2015

*Keywords:*
DRENAR
BABA
Dipolar coupling
Double quantum excitation

ABSTRACT

A new pulse sequence entitled DQ-DRENAR, (**D**ouble-**Q**uantum based **D**ipolar **R**ecoupling **E**ffects **N**uclear **A**lignment **R**eduction) was recently described for the quantitative measurement of magnetic dipole–dipole interactions in homonuclear spin-1/2 systems involving multiple nuclei. The double quantum coherences were created via a windowless symmetry-based pulse sequence (POST-C7). The present contribution evaluates the performance of the "Back-to-Back" excitation pulse scheme BABA-xy16 in such DRENAR experiments. Using SIMPSON simulations, special attention is given to finite pulse length effects, dipolar truncation, and chemical shift anisotropy interference. Experimental results on model compounds demonstrate good stability up to long mixing times ( $>10$ ms) as well as high accuracy. As its dipolar coupling efficiency is relatively high (the dipolar coupling scaling factor is 4.24 times as high as that of POST-C7), DQ-DRENAR-BABA-xy16 is most appropriate for the measurement of relatively weak dipolar coupling strengths ( $<400$ Hz). Different from POST-C7, for which the spinning rate is limited to 1/7 of the nutation frequency, DQ-DRENAR-BABA-xy16 experiments can take full advantage of ultrafast MAS experiments.



## 1. Introduction

Because of their straightforward relationship to inter-nuclear distance geometry, and bond connectivity, magnetic dipole–dipole coupling information is one of the principal targets of solid state nuclear magnetic resonance (SSNMR) experiments [1–5]. While simple static experiments such as Hahn spin-echo decay [6–9] and spin-echo double resonance (SEDOR) spectroscopies [10] afford such information as well, the combination with magic-angle spinning (MAS) is much more powerful as it allows this information to be obtained in a site-resolved fashion. As previously discussed, the homonuclear dipolar coupling interaction can be re-introduced into the MAS Hamiltonian by applying appropriate re-coupling schemes while preserving the high resolution afforded by MAS [11–15].

Compared to the site-resolved measurement of heteronuclear dipole coupling by dipolar recoupling methods such as REDOR [5], the homonuclear case is substantially more complex, both from a theoretical and an experimental standpoint, especially when multi-spin interactions are encountered. Specifically, dipolar truncation phenomena influence the otherwise straightforward effect of the distance geometry upon the experimental observables [16–18] and the separation of dipolar interaction and chemical shift anisotropy effects is sabotaged by intractable cross-terms involving both interactions [19]. Because of these complications, calibration procedures used to compensate for experimental imperfections are often valid only for specific situations and are thus not generally applicable. As a result, among the numerous homonuclear dipolar recoupling methods that have been developed [20–25]; no clear method of choice can be identified. A powerful approach of homonuclear re-coupling is based on the excitation of double quantum coherences using suitable excitation strategies [26–33]. One interesting variant in this context is the DQ-DRENAR method developed in our laboratory [32,33], which accomplishes recoupling by means of a POST-C7 sequence. The sequence consists of two DQ-excitation blocks, which result in attenuating the z-magnetization, which is then detected by a simple 90° pulse (signal intensity $S$'). A reference signal $S°$ with the dipolar recoupling absent is generated by shifting the phase of the second DQ excitation block by 90° relative to the first block. In analogy to the REDOR approach, the homonuclear dipole–dipole coupling constant can then be easily extracted from a plot of the

* Corresponding author.
*E-mail addresses:* renjinjunsiom@163.com (J. Ren), eckerth@uni-muenster.de (H. Eckert).

http://dx.doi.org/10.1016/j.ssnmr.2015.10.007
0926-2040/

normalized difference signal ($S°–S'$)/$S°$ versus dipolar mixing time. In contrast to the related method of double-quantum excitation spectroscopy [27,28], DRENAR measures the decay of longitudinal magnetization as a function of dipolar mixing time. While DQ-DRENAR has proven a robust method for homonuclear dipolar coupling measurements, the DQ excitation using windowless pulses suffers from certain practical limitations regarding the spinning rate and mixing times, which are associated with the boundary conditions of the POST-C7 pulse block (the nutation frequency has to be 7 times the spinning rate and the pulses are windowless during the whole mixing time). As suggested by Saalwächter [34], results of equivalent quality should be obtainable using Back-to-Back (BABA) DQ- excitation. The effects of CSA and resonance offsets upon the performance of DRENAR in relation to DQ-excitation spectroscopy was discussed on the basis of detailed simulations, however, no experimental results were presented. Here we will give a detailed discussion of DQ-DRENAR with BABA excitation, from the theoretical, simulation, and experimental perspectives.

## 2. Theoretical background

The theory of DQ-DRENAR has been described in Ref. [33]. The DQ-DRENAR-BABA-xy16 sequence discussed in the present manuscript is shown in Fig. 1. The pulse blocks of (a) and (b) are BABA-xy16 and an additional modified version, respectively. In the modified version, two pulse blocks are added before the normal DQ-DRENAR-BABA-xy16 sequence; in the $S'$ part, the phase of pulse block 2 alternates between 0 and $\pi$. Both DQ-DRENAR-BABA-xy16 and the modified one can generate the data points every 16 rotor periods. However, their data points have 8 rotor period shifts. Therefore, by combining DQ-DRENAR-BABA-xy16 and the modified one, the data step can be reduced to 8 rotor periods. By combining BABA-xy16 and its modification, the increment of the mixing time can be decreased from normally 16 rotor periods to 8 rotor periods. In DRENAR, the dipolar recoupling effected by this DQ-Hamiltonian results in a diminution of the longitudinal magnetization, whose amplitude ($S'$) is then detected with a 90° reading pulse. In the referencing experiment, all pulses during the second half of the mixing time are rotated by 90° resulting in no recoupling of the magnetic dipolar interaction. Again, the amplitude of the longitudinal magnetization ($S_0$) is then measured as a function of mixing time. Owing to the difference method used, some unwanted decay owing to relaxation effects is eliminated.

In a spin system containing two spin-1/2 nuclei, BABA is represented by the Hamiltonian [35]:

$$\bar{H}^0 = d_{jk}(T^{jk}_{22} + T^{jk}_{2-2}) \tag{1a}$$

where $T^{jk}_{22} = \frac{1}{2}I^+_j I^+_k$ and $T^{jk}_{2-2} = \frac{1}{2}I^-_j I^-_k$ are the irreducible dipolar tensor operators representing double quantum transitions, and $d_{jk}$ are orientation dependent coefficients related to the dipolar coupling constant between spins $j$ and $k$, $b_{jk}$, according to:

$$d_{jk} = \frac{3}{\pi\sqrt{2}} b_{jk} \sin 2\beta \sin\gamma \tag{1b}$$

where $\gamma$ and $\beta$ are the Euler angles relating the principal axis system of the dipolar coupling tensor to the rotor fixed frame.

The evolution of longitudinal magnetization $I_{jz}+I_{kz}$, under the double quantum Hamiltonian is then given by:

$$(I_{jz} + I_{kz})_{t=NT_r} \underset{\bar{H}^0}{\rightarrow} (I_{jz} + I_{kz})_{t=0} \cos(d_{jk} NT_r) + \left[ i\left(I^+_j I^+_k - I^-_j I^-_k\right)\right] \sin(d_{jk} NT_r) \tag{2}$$

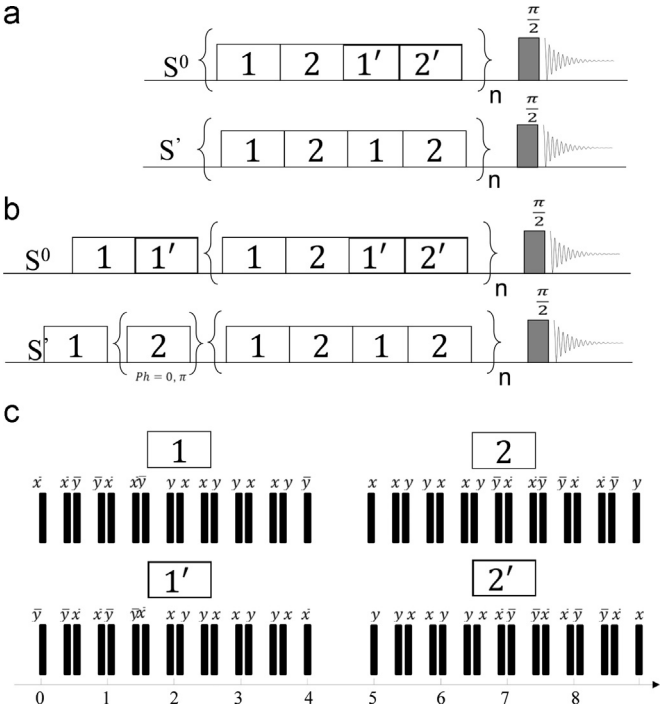


**Fig. 1.** (a) Standard DQ-DRENAR-BABA-xy16: the combination of pulse block 1 and 2 constitutes the BABA-xy-16 sequence; all the pulses within blocks 1′ and 2′ are 90° shifted relative to the blocks 1 and 2, respectively. The S° reference signals are obtained by combining the BABA-xy16 and 90° shifted BaBA-xy16 to average out the dipolar coupling effect. S' is obtained by repeating the unshifted BABA-xy16 block to recouple the dipolar interaction. (b) Modified sequence (see text); (c) the construction of the pulse block, corresponding to phases 1, 2, 1′ and 2′.

The relative observed average signal amplitude over all orientations after the final 90° pulse for creating single quantum coherence is given by:

$$S'_{(t=NT_r)} = \int_{\gamma=0}^{2\pi}\int_{\beta=0}^{\pi} \frac{\cos(d_{jk}NT_r) r \sin\beta d\gamma r d\beta}{4\pi r^2} \tag{3}$$

Using the expansion

$$\cos x = 1 - \frac{x^2}{2!} + \frac{x^4}{4!} \pm \ldots \tag{4}$$

and truncating the latter after the second term in the limit of $x = |d_{jk}|NT_r \leq 1$, results in a first-order approximation of the dephasing

$$\frac{S_0 - S'}{S_0}_{(t=NT_r)} = \downarrow \frac{1}{8\pi}\int_{\gamma=0}^{2\pi}\int_{\beta=0}^{\pi} (d_{jk}NT_r)^2 \sin\beta d\beta d\gamma = \downarrow \frac{1}{8\pi} * \frac{9}{2\pi^2}\frac{16\pi}{15} * (4\pi^2)(b_{jk}NT_r)^2 = \frac{12}{5}(b_{jk}NT_r)^2 \tag{5}$$

For a three-spin system, similar as with DQ-DRENAR-POST-C7, the normalized dephasing effect is given by:

$$\frac{S_0 - S'}{S_0}_{(t=NT_r)} = \frac{|d_{jk}|^2 + |d_{ji}|^2}{|d_{ik}|^2 + |d_{jk}|^2 + |d_{ji}|^2}\left(1 - \cos\left(\sqrt{\left(|d_{ik}|^2 + |d_{jk}|^2 + |d_{ji}|^2\right)}NT_r\right)\right) = a\left(1 - \cos\left(\sqrt{\left(|d_{ik}|^2 + |d_{jk}|^2 + |d_{ji}|^2\right)}NT_r\right)\right)_{(t=NT_r)} \tag{6}$$

Whereas for a treatment of the three-spin interaction in terms of a summation of three two-spin interactions the equation would be:

$$\frac{S_0 - S'}{S_0}_{(t=NT_r)} = \left(1 - \cos\left(\sqrt{\left(|d_{ik}|^2 + |d_{jk}|^2 + |d_{ji}|^2\right)}NT_r\right)\right) \quad (7)$$

The comparison between (6) and (7) reveals the pre-factor $a$, which scales the dephasing effect. When $|d_{ik}|^2 \gg |d_{jk}|^2 + |d_{ji}|^2$, the dephasing effect affecting the signal of the observed spin j is strongly diminished (dipolar truncation effect [16–18]).

After powder averaging and first order approximation of $\cos(\sqrt{(|d_{ik}|^2 + |d_{jk}|^2 + |d_{ji}|^2)}NT_r)$, the observed normalized dephasing is calculated from the expression

$$\frac{S_0 - S'}{S_0}_{(t=NT_r)} = \frac{12}{5}\left(\sqrt{\left(\sum_k b_{jk}^2\right)}NT_r\right)^2 \quad (8)$$

Thus, in multiple-spin systems, an effective dipolar coupling consnt $b_{jk}$ can be defined as

$$b_{jk}^{eff} = \sqrt{\left(\sum_k b_{jk}^2\right)}$$

where the symbol $k$ denotes all the spins coupled to spin j.

Thus, compared with the dephasing effect of DQ-DRENAR-POST-C7 [33],

$$\frac{S_0 - S'}{S_0}_{(t=NT_r)} = \frac{0.86\pi^2}{15}\left(\sqrt{\left(\sum_k b_{jk}^2\right)}NT_r\right)^2 \quad (9)$$

DQ-DRENAR-BABA has a ~4.24 times higher scaling factor regarding excitation strength. Therefore BABA is expected to be particularly useful for measuring very weak dipolar coupling effects.

## 3. Results and discussion

### 3.1. Simulations

Fig. 2 shows the attenuation curve for isolated two-spin-1/2 systems simulated using the SIMPSON program package [36]. The normalized dephasing consists of an initial build-up region followed by an oscillatory part. In principle, the dipolar coupling constant can be measured accurately by simulating the oscillatory part at long dipolar mixing times. However, in disordered systems, the internuclear distance and the dipolar constants are not singular values, but are subject to some distribution effects. As a result, the oscillations are damped or not even observed in such systems. Similar damping effects occur as a result of secondary inter-pair interactions at longer distance ranges. For these reasons, it appears more useful to estimate the dipolar coupling information from the initial dephasing at short mixing times. From (9), it can be found that by fitting the initial data range to a parabola, the square of the effective dipolar constant, $b_{jk}^{eff}$, can be obtained. Clearly, this approximation results in a systematic underestimation effect, which gets more serious with increasing fitting range. Fig. 2b shows that, independent of the spin geometry, this error is contained within the random error threshold of 10–15% if data analysis is limited to the data range $\frac{(S_0 - S')}{S_0} \leq 0.4$–$0.5$. If in the absence of dipolar truncation effects – the parabolic analysis can be carried out within this particular data range, Fig. 2b shows that we can account for this systematic error by means of the calibration factor $f_a \sim 0.875$.

It should be noted that beside the first order approximation, the finite 90° pulse length (as opposed to an infinitely short one) during the rotor cycle also results in a systematic underestimation of the effective dipolar coupling strength. With increasing duty cycle (ratio of pulse length to half rotor period), both the normalized dephasing rate and apparent $b_{jk}^2$ value obtained by parabolic fitting (see Fig. 3) of the simulated data decrease. This kind of underestimation can be approximated by the universal empirical expression:

$$\frac{\Delta b_{jk}^2}{b_{jk}^2} = -2.53 \times \left(\frac{\text{pulse length}}{\text{half rotor period}}\right)^2 \quad (10)$$

where $\Delta b_{jk}^2 = b_{jk}^2(\text{true}) - b_{jk}^2(\text{apparent})$, $b_{jk}^2 = b_{jk}^2(\text{true})$. Because such errors can be quantitatively predicted, we can use a calibration factor $f_p$ to correct such underestimation. This calibration factor can be defined as:

$$f_p = 1 - 2.53 \times \left(\frac{\text{pulse length}}{\text{half rotor period}}\right)^2 \quad (11a)$$

$$b_{jk}^2(\text{true}) = b_{jk}^2(\text{apparent})/f_p \quad (11b)$$

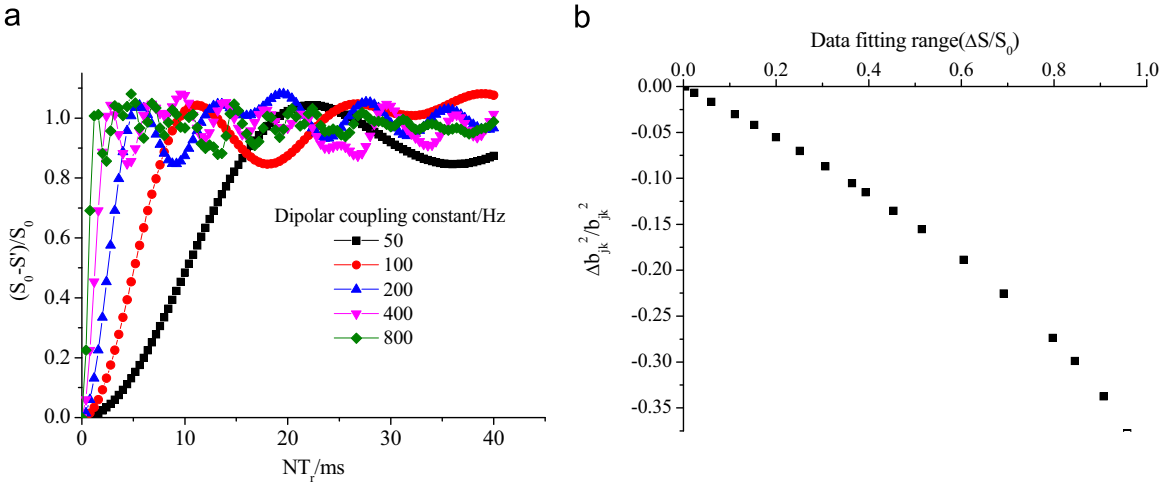


**Fig. 2.** Simulated 2-spin DQ-DRENAR-BABA-xy16 curves and error analysis. (a) The curves are simulated, assuming $b_{jk}$=50, 100, 200, 400, 800 Hz and $\nu_r$=40 kHz, respectively; (b) the normalized systematic error (deviation $\Delta b_{jk}^2/b_{jk}^2$ of the estimated $b_{jk}^2$ value from the true value) using the parabolic fitting approximation. Extremely short pulses (90° pulse length of 0.1 μs) are assumed.

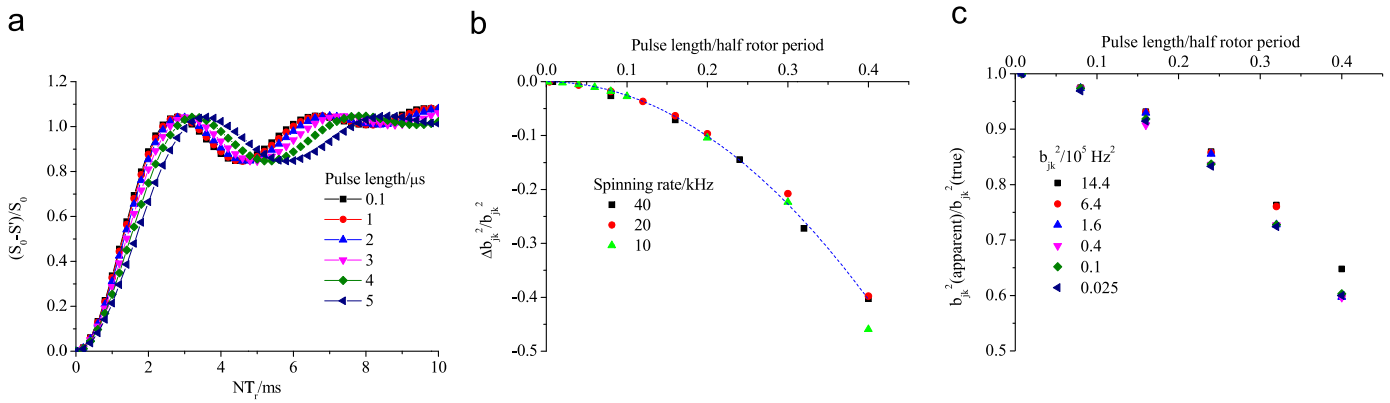


**Fig. 3.** Systematic error resulting from finite pulse lengths in BABA-DRENAR. (a) Simulated two-spin DQ-DRENAR-BABA-xy16 and modified DQ-DRENAR-BABA-xy16 data curves with different 90° pulse lengths, assuming $b_{jk}$=400 Hz, $\nu_r$=40 kHz, respectively. (b) The systematic error of $b_{jk}^2$ value caused by finite 90° pulse length at different spinning rates. The blue dashed curve shows a fit to the correlation of the normalized underestimation ( $\Delta b_{jk}^2/b_{jk}^2$ ) that would result by making a parabolic fit to the experimental data within $\Delta S/S_0$ against the ratio of (pulse length)/(half rotor period). Simulation results for different dipolar coupling strengths are included. (c) Plot of $f_P$ (see text) as a function of duty cycle (pulse length per half rotor period) for different magnitudes of. (For interpretation of the references to color in this figure legend, the reader is referred to the web version of this article.)

where $b_{jk}^2$(true) and $b_{jk}^2$(apparent) are the correct and the apparent $b_{jk}^2$ values, respectively. Here, the apparent value is the one obtained by fitting the experimental data to a parabola, following Eq. (8). Fig. 3 shows that up to duty cycles of 20% the systematic finite pulse length error is comparable to the random error of the measurement. Furthermore, the calibration factor is essentially independent of the magnitude of the dipolar coupling strength.

As discussed above, DQ-DRENAR-BABA-xy16 can be easily extended to multiple spin systems. Fig. 4, left, shows the simulated data curves for $I_j(I_k)_n$ systems at equal distances in a pseudo-tetrahedral geometry. With increasing $n$, the dephasing effect and the oscillation frequency increase as expected. By parabolic fitting or SIMPSON simulation of the initial data range, the quantity $\sum_k b_{jk}^2$ can be estimated according to Eq. (8). In addition, multiple-spin systems will be affected by dipolar truncation effects (see Fig. 4, right), necessitating more limited fitting or simulation ranges to avoid large systematic errors in the $\sum_k b_{jk}^2$ values extracted from such curves.

The CSA always interferes with an accurate measurement of the homonuclear dipolar coupling. Fig. 5 shows the simulated data curves obtained for DQ-DRENAR-BABA-xy16 and its modified version. Contrary to the situation with DQ-DRENAR-POST-C7, CSA interference effects behave in a more straightforward fashion: the dipolar coupling constant is monotonically underestimated, and the sign of the CSA (positive or negative) makes no difference with regard to the measured DRENAR curve. Note also that very high spinning rates can diminish the effect of the CSA, an option which is not normally available with POST-C7 excitation schemes. Since the BABA-xy16 and its modification respond to the CSA in different ways, the combination of both data sets leads to some dispersal of the data acquired with the standard and the modified scheme, especially when mixing times are long and csa-s are large (see simulated data for CSAs of 28 and 35 kHz in Fig. S1, Supplementary information). Fig. 5c shows that for a given magnitude of the dipolar coupling constant, the underestimation of $b_{jk}^2$ is universally dependent on the ratio $(\frac{\text{CSA}}{\text{spinning rate}})^2$ and that this relationship is

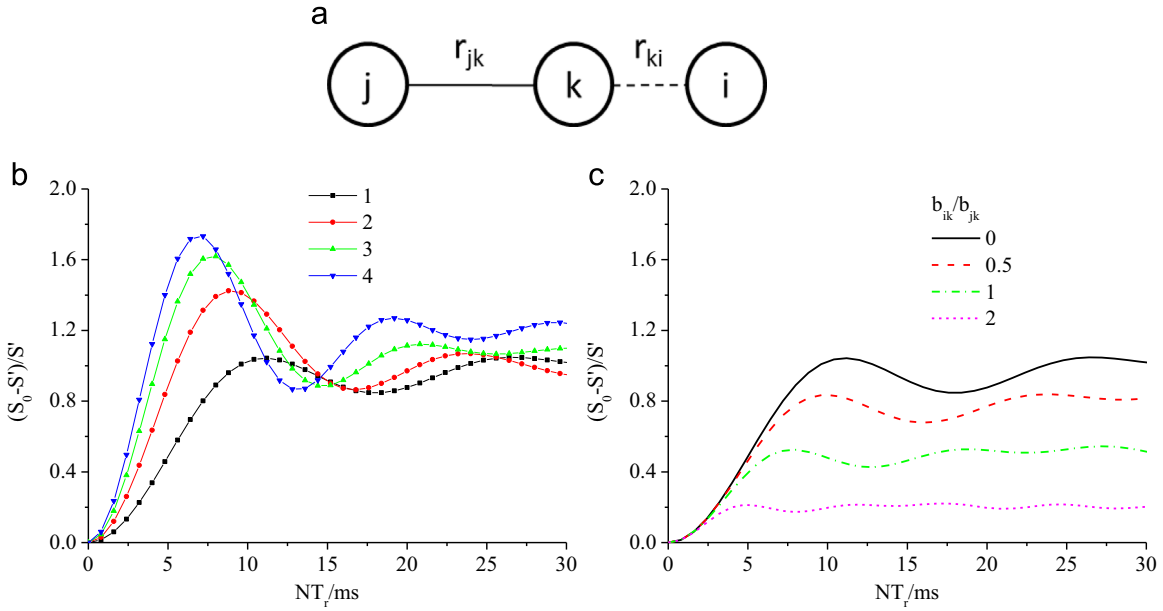


**Fig. 4.** Left: Simulated DQ-DRENAR curves for an $I_j(I_k)_n$ spin system in a pseudo-tetrahedral geometry; $n$=1, 2, 3 and 4; spin j is coupled to $n$ spins k; the interaction between spins k is taken into account, assuming $b_{jk}$= 100 Hz, $\nu_r$=20 kHz, respectively. Right: Dipolar truncation effects evident from simulated DRENAR curves for a linear three-spin system, where the observe spin j is coupled to spin k, which is also coupled to spin i; $b_{ik}/b_{jk}$=0, 0.5, 1, and 2, respectively, assuming $b_{jk}$=100 Hz, and $\nu_r$=20 kHz, respectively. Extremely short pulses (90° pulse length of 0.1 μs) are assumed.

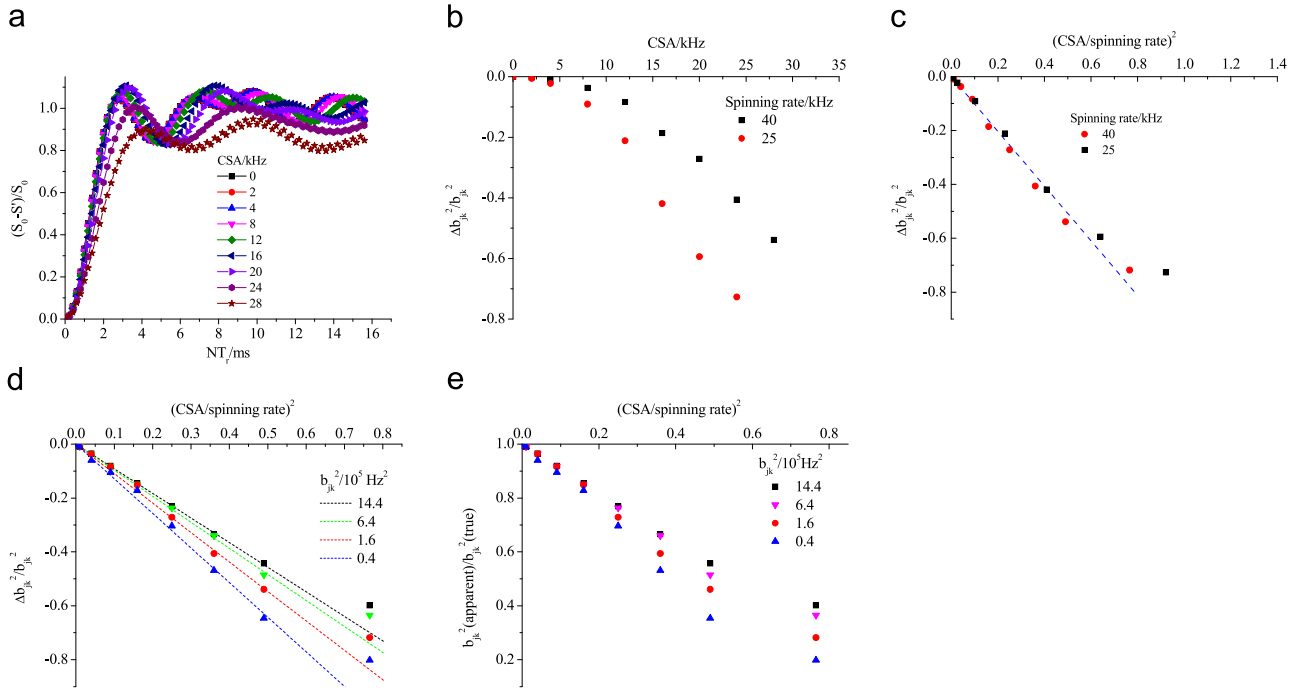


**Fig. 5.** (a) Simulated DRENAR curves of a 2-spin system with different CSA values, obtained by combining the data from DQ-DRENAR-BABA-xy16 and modified DQ-DRENAR-BABA-xy16, assuming $b_{jk}$=400 Hz, and $\nu_r$=40 kHz, respectively. To avoid the effect of pulse length, the 90° pulse length is set to be 0.1 μs. All the parabola fitting range is ≤0. 5. (b) The underestimation of $b_{jk}^2$ under the effect of CSA at two different spinning speeds. (c) The underestimation of $b_{jk}^2$ as a function of $(\frac{\text{CSA}}{\text{spinning rate}})^2$, assuming a dipolar coupling constant $b_{jk}$=400 Hz, at two different spinning speeds. The blue dashed curve shows the linear fitting regime within the range of $(\frac{\text{CSA}}{\text{spinning rate}})^2 \le 0.5$. (d) The underestimation of $b_{jk}^2$ as a function of $(\frac{\text{CSA}}{\text{spinning rate}})^2$ for different dipolar coupling strengths $b_{jk}^2$ = 0.4, 1.6, 6.4, and 14.4×10$^5$ Hz, respectively; simulated for a spinning rate $\nu_r$=40 kHz. The dashed curves denote the linear regimes, using the function $\frac{\Delta b_{jk}^2}{b_{jk}^2} = a \times (\frac{\text{CSA}}{\text{spinning rate}})^2$, where the value of $a$ is weakly dependent on the dipolar coupling strength. (e) Dependence of $f_c$ on $(\frac{\text{CSA}}{\text{spinning rate}})^2$ and $b_{jk}{}^2$; $\nu_r$ =40 kHz. (For interpretation of the references to color in this figure legend, the reader is referred to the web version of this article.)

linear up to $(\frac{\text{CSA}}{\text{spinning rate}})^2$=0.5. However, because of the cross terms involved, moderately different scaling curves are observed for different dipolar coupling strengths (Fig. 5d). The systematic errors become less severe for larger dipolar coupling strengths. Based on these simulation results, we can correct for this underestimation by means of a calibration factor $f_c$, to be determined by roughly estimating the dipolar coupling strength from the experimental data.

$$f_c = 1 + a \times \left(\frac{\text{CSA}}{\text{spinning rate}}\right)^2 \tag{12a}$$

$$b_{jk}^2(\text{true}) = b_{jk}^2\big(\text{apparent}\big)/f_c \tag{12b}$$

where $a$ is the slope of the linear function. From Fig. 5d we find $a$=−1.285, −1.093, −0.967, and −0.913, respectively, for the $b_{jk}^2$(true)=0.4, 1.6, 6.4 and 14.4 ×10$^5$ Hz$^2$. The appropriate factor $f_c$ can thus be used to correct for CSA effects. Not unexpectedly, this calibration factor depends not only on the ratio of csa/spinning rate, but also on the strength of the magnetic dipole–dipole coupling (see Fig. 5e). When $(\frac{\text{CSA}}{\text{spinning rate}})^2$ exceeds 0.5, the correction is going to be less reliable, owing to the data dispersal effect observed in the combination of the regular and the modified BABA-DRENAR sequences (Fig. S1).

Aside from these details the characteristics of DQ-DRENAR-BABA-xy16 are found to be quite similar to those of DQ-DRENAR-POST-C7 because of the common properties of the DRENAR principle involved. Because of its simpler excitation scheme, BABA may be expected to give more stable data at differing spinning rates and at longer mixing times than POST-C7.

### 3.2. *Validation on model compounds*

The performance of DQ-DRENAR-BABA-xy16 has been tested on seven samples containing 16 different sites, covering a wide range of dipolar coupling strengths. Fig. 6 compares the experimental data with the corresponding simulated curves. The latter were obtained with the SIMPSON code based on the crystallographic distances, accounting for both finite pulse lengths under the experimental conditions (rotor speeds) applied. In the simulation, all the standard samples except crystalline $Na_5P_3O_{10}$ are assumed to be two-spin systems with an effective internuclear distance calculated from the $\sum_k b_{jk}^2$ values from the crystal structure extending over a distance range of 3-times the closest distance between coupled nuclei. In crystalline $Na_5P_3O_{10}$ the calculation is based on three-spin systems formed by the phosphate trimeric units. In addition the effects of CSA are included in the simulations. Parabolic fits to these simulated curves were conducted within the data range $\Delta S/S^\circ < 0.2$–0.5 (depending on the magnitude of dipolar truncation effects) and the corresponding $\Sigma b_{jk}{}^2$ values extracted from these curves are given in column d of Table 1. The compound $CdPS_3$ (Fig. 6a) presents the most straightforward case of an isolated two-spin system with a rather strong dipolar interaction across a short (2.223 Å) internuclear

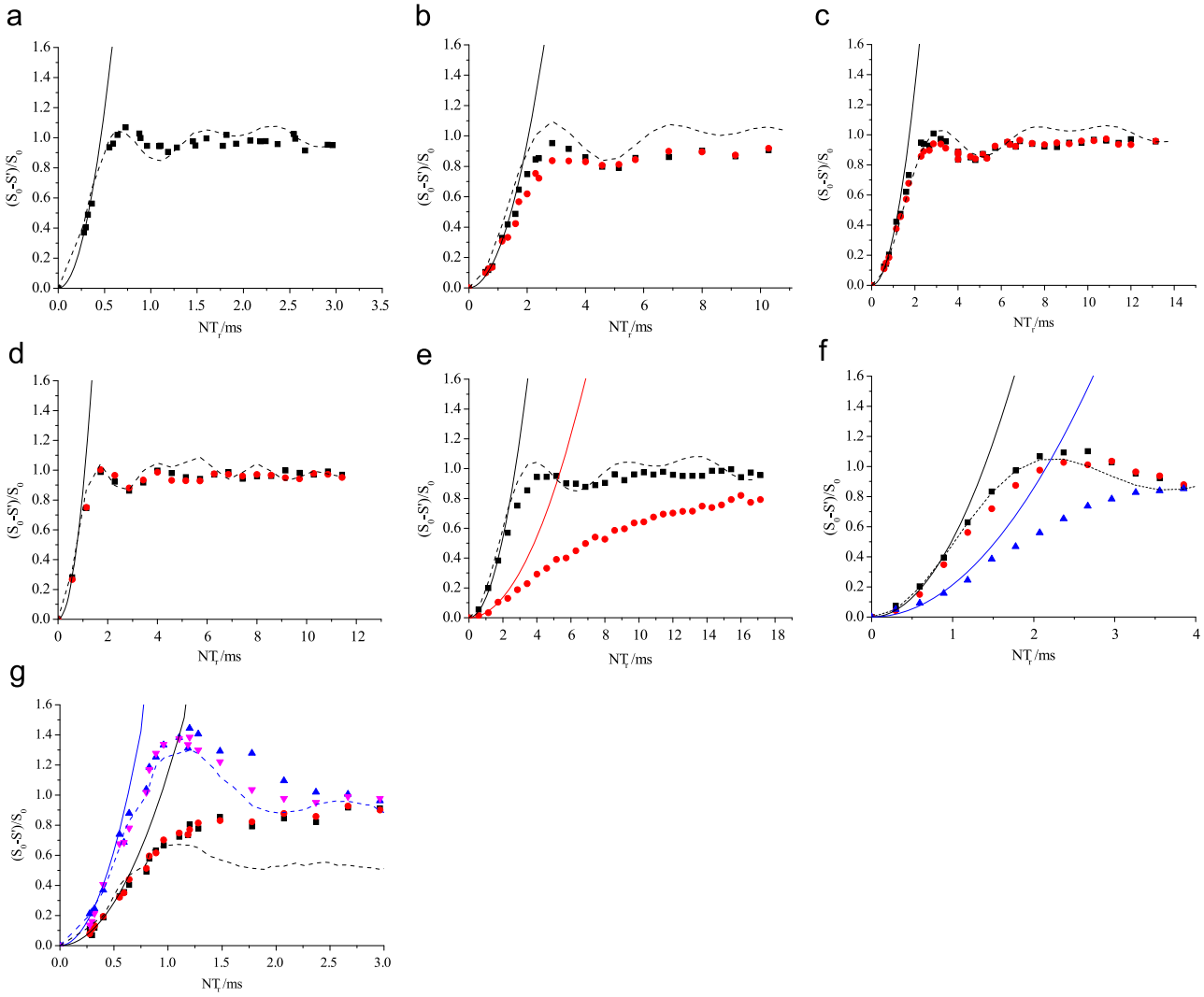


**Fig. 6.** Experimental and simulated DQ-DRENAR-BABA-xy16 curves. Dashed curves show simplified spin cluster simulations based on $\sum_k b_{jk}^2$ values from the crystal structures and taking the effects of finite pulse length and CSA into account. Solid curves are parabolic approximations based on Eq. (8) to the experimental curves, resulting in the $\sum_k b_{jk}^2$ values listed in Table 1, column d. (a) $CdPS_3$; (b) P, P-[3] ferrocenophane 1: the black squares and red circles represent the signal at 16.6 and −27.7 ppm respectively; (c) P, P-[3] ferrocenophane 5: the black squares and red circles represent the signal at 6.3 and −26.3 ppm respectively; (d) P, P-[3] ferrocenophane 6: red circles and black squares represent the signals at −20.9 ppm, and -3.8 ppm respectively; (e) $Li_{13}Si_4$: black squares and red circles represent the $^{29}Si$ signals at 263.4 and 220.7 ppm, respectively; (f) $Ag_7P_3S_{11}$: blue triangles, red circles and black squares represent the signals at 103.2 ppm, 101.4 ppm and 92.0 ppm, respectively (g): $Na_5P_3O_{10:}$ red circles and magenta triangles represent the signal from $Q^1$ (1.3 ppm) and $Q^2$ units (−7.4 ppm) of phase I, respectively; black squares and blue triangles represent the $Q^1$ (4.9 ppm) and $Q^2$ units (−5.8 ppm) of phase II, respectively. (For interpretation of the references to color in this figure legend, the reader is referred to the web version of this article.)

distance. Likewise, the P,P-ferrocenophanes can be approximated as two-spin systems having variable distances as described in Ref. [40]. Fig. 6b–d illustrates that these differences are well-resolved by our DQ-DRENAR-BABA experiments. For all four compounds the oscillatory parts of the DRENAR curves are in excellent agreement with those expected from the crystallographic internuclear distances. Also, the parabolic approximation of the initial data range up to $\frac{S_0-S'}{S_0}$=0.4–0.5 leads to a satisfactory agreement of the experimental dipolar coupling constants with those expected from the crystal structures. Fig. 6e shows results on a $^{29}Si$ enriched (99.34%) sample of $Li_{13}Si_4$. This compound contains two crystallographically distinct silicon sites in a 1:1 ratio: a dimeric $Si_2^{6-}$ species with an internuclear distance of 2.378 Å (Si-1 site, 263.4 ppm) and a monomeric $Si^{4-}$ species (Si-2 site, 220.7 ppm). Clearly, DQ-DRENAR is able to resolve the large difference in dipolar coupling strength between both silicon sites. Also, clear dipolar truncation effects are evident for the DQ-DRENAR curve of the monomeric Si-2 species, as these nuclei experience dipolar coupling to the dimeric Si-1 species, which are strongly coupled among each other, owing to the short Si–Si distance in this dimeric $Si_2^{6-}$ unit.

Crystalline $Ag_7P_3S_{11}$ has three different $^{31}P$ sites, giving rise to three distinct signals. The signal at 103.2 ppm comes from isolated $[PS_4]^{-3}$ ions, while the other two signals at 101.4 ppm and 92.0 ppm result from a pyrothiophosphate dimer, with a P–P distance of 3.607 Å. As illustrated by Fig. 6f, the large difference in dipolar coupling between these two types of P atoms is well resolved by the BABA-DRENAR experiment. For the isolated $^{31}P$ sites (103.2 ppm), the dipolar truncation effect is again clearly evident, as also previously reported for DRENAR-POST-C7 experiments [33]. Finally, Fig. 6g shows the results for the two spectroscopically resolved crystalline phases of anhydrous $Na_5P_3O_{10}$. Both of these phases have trimeric repeat units. The middle P in the trimer is a $Q^2$ unit, which connects with two terminal P ($Q^1$ units) through P–O–P linkages. As expected the $Q^2$ units show a much stronger dephasing effect than the $Q^1$ units. Also the DRENAR curves for the $Q^1$ species show some indication of dipolar truncation effects, and

**Table 1**
$^{31}$P isotropic chemical shifts ( ± 0.5 ppm), CSA values ( ± 5 ppm), crystallographic (column a) and experimental (column b) distances between closest coupled nuclei in a range of phosphorus-containing model compounds. Also listed are the $\sum_k b_{jk}^2$ values obtained by SIMPSON simulation (column c), the apparent $\sum_k b_{jk}^2$ values obtained by parabolic fitting of the experimental data without any corrections (column d), $\sum_k b_{jk}^2$ values after first order approximation, pulse length and CSA correction (column e) and theoretical $\sum_k b_{jk}^2$ values calculated according to the crystal structure (column f). CSAs are defined according to $\Delta\sigma = \frac{2\sigma_{ZZ} - (\sigma_{XX} + \sigma_{YY})}{3}$.

| Sample | $\delta_{iso}$/ppm | CSA/ppm | $D_{cry}$/Å | $D_{exp}$/Å | $\sum_k b_{jk}^2/10^5$ Hz$^2$( ± 10%) | | | |
|---|---|---|---|---|---|---|---|---|
| | | | a | b | c | d | e | f |
| P, P-[3] ferrocenophane 1 | 16.6 | 47 | 3.653 | 3.653 | 1.64 | 1.0 | 1.40 | 1.64 |
| | −27.7 | −45 | 3.653 | 3.653 | 1.64 | 0.87 | 1.20 | 1.64 |
| P, P-[3] ferrocenophane 5 | 6.3 | −32 | 3.601 | 3.50 | 2.12 | 1.37 | 1.72 | 1.78 |
| | −26.3 | −44 | 3.601 | 3.50 | 2.12 | 1.22 | 1.67 | 1.78 |
| P, P-[3] ferrocenophane 6 | −3.8 | −49 | 3.052 | 3.150 | 3.98 | 3.58 | 4.98 | 4.81 |
| | −20.9 | −38 | 3.052 | 3.150 | 3.98 | 3.40 | 4.40 | 4.81 |
| $CdPS_3$ | 103.3 | 26 | 2.223 | 2.286 | 27.2 | 19.75 | 25.2 | 33.3 |
| $Ag_7P_3S_{11}$ | 103.2 | −15 | n.m. | n.m. | n.m. | 0.89 | 1.06 | 1.15 |
| | 101.4 | −50 | 3.607 | 3.427 | 2.40 | 1.83 | 2.30 | 2.79 |
| | 92.0 | 40 | 3.607 | 3.339 | 2.81 | 2.15 | 2.65 | 2.81 |
| $Na_5P_3O_{10}$ (I) | 1.3 | −96 | 2.866 | 2.783 | 8.40 | 5.1 | 7.32 | 9.79 |
| | −7.4 | 127 | 2.866 | 2.80 | 16.1 | 8.1 | 13.7 | 16.1 |
| $Na_5P_3O_{10}$ () | 4.9 | −107 | 2.867 | 2.783 | 8.40 | 4.8 | 7.24 | 10.1 |
| | −5.8 | 116 | 2.967 | 2.80 | 16.1, | 10.5 | 16.6 | 16.1 |
| $Li_{13}Si_4$ | 263.4 | 48 | 2.378 | 2.432 | 1.09 | 0.56 | 0.86 | 1.50 |
| | 220.7 | 128 | n.m. | n.m. | n.m. | 0.14 | 0.33 | 0.31 |

[a]Crystallographic distance between closest coupled nuclei.
[b]Distance between closest coupled nuclei estimated by simulation from DQ-DRENAR-BABA-xy16 and its' modification (according to the sum of squared dipolar coupling constants).
[c, d] $\sum_k b_{jk}^2$ values estimated by simulation from DQ-DRENAR-BABA-xy16 and its modification, and parabola fitting of experimental data without any correction.
[e] $\sum_k b_{jk}^2$ values obtained by correcting the values in column c in the form of $\sum_k b_{jk}^2$(column d)/($^f$f$^*$f$_p$$^*$f$_c$ ).
[f]Theoretical $\sum_k b_{jk}^2$ values calculated according to the crystal structure extending over a distance range of 3-times the closest distance between coupled nuclei.
n.m. not measured.

thus the data range for the parabolic analysis needs to be more restricted. Notably, the dipolar coupling constants in this three-spin system are reasonably well reproduced by the experiment, despite the relatively large chemical shift anisotropy. The simulation data curves are very close to the experimental data even at long mixing times, which proves that the sequence performs very robustly under the conditions applied. Table 1 also compares the simulated values of $\Sigma b_{jk}^2$ with apparent values (column d), resulting from direct parabolic fitting of the experimental data without any correction. Clearly such a simplified procedure produces unsatisfactory results in many situations where duty cycles are high and csa-s are large. However, with the pulse lengths and spinning speeds under experimental control, and approximate CSA information available from suitable experimental schemes, it will always be possible to correct such experimental data with the help of the calibration factors shown in Figs. 3(c) and 5(d), Eqs. (11) and (13), i.e. by using the three calibration factors $f_a$, $f_p$ and $f_c$, according to the expression:

$$\sum_k b_{jk}^2\left(\text{true}\right) = \sum_k b_{jk}^2\left(\text{apparent}\right)/\left(f_a f_p f_c\right). \quad (13)$$

This possibility is particularly valuable for the structural analysis of disordered or glassy materials, for which no rigorous SIMPSON simulations can be carried out in the absence of crystallographic information on the applicable spin geometries. After calculating the calibration factors according to Fig. 2b, Eqs. 11 (a) and 12(a), accurate dipolar coupling values can be obtained, according to Eq. (13).

## 4. Conclusions

As shown by detailed SIMPSON simulations and experimental model compound work in the present study, the robust Back-to-Back (BABA)-xy16 excitation scheme is a viable alternative to the windowless POST-C7 pulses in DQ-DRENAR experiments. The results demonstrate good stability up to long mixing times as well as high accuracy. As its dipolar scaling factor is 4.24 times as high as that of POST-C7, DQ-DRENAR-BABA-xy16 is most appropriate for the measurement of relatively weak dipolar coupling strengths. It can also be expected to accurately measure the geometry of isolated multiple spin systems from the oscillatory behavior at long mixing times. Finite pulse length effects and chemical shift anisotropies will result in an underestimation of dipolar coupling strengths, but their influences upon the data can be included in the simulations and/or accounted for by calibration factors in the parabolic analysis of data within the initial range $\Delta S/S^\circ < 0.5$. Unlike the POST-C7 excitation scheme, the BABA DQ-excitation poses no limits on MAS-spinning speeds, as there is no fixed relation between nutation frequency and spinning speed. Thus, the advantages of ultra-fast MAS (including the minimization of CSA effects) can be realized in this case. Finally, owing to the simpler DQ-excitation scheme, DQ-DRENAR-BABA-xy16 is expected to have better performance than DQ-DRENAR-POST-C7 in older spectrometers with lower pulse programmer switching speeds.

## 5. Experimental details

$Ag_7P_3S_{11}$, and $CdPS_3$ are prepared according to literature procedures [37,38]. $Na_5P_3O_{10}$ hydrate was obtained from Aldrich Chemicals and dried at 250 for 24 h to remove the crystal water before the measurement. After heating at 250 degree, it is mixture of two phases [39]. Three P,P-[3] ferrocenophanes were obtained from collaborators; their NMR characterization is described in Ref. [40]. The preparation and NMR characteristics of the $^{29}$Si enriched sample of $Li_{13}Si_4$ is described in Ref. [41]. $^{31}$P experiments were done on a Bruker Avance III 300 spectrometer. The DQ-DRENAR-

BABA-xy16 and its modification experiments were carried out with a 2.5 mm probe operating at spinning rates between 20 and 29 kHz. For the P, P-[3] ferrocenophanes and $Li_{13}Si_4$ samples, measurements were conducted with a 4 mm probe operating at spin rates between 10.0 and 14.0 kHz. The $^{31}P$ 90° pulse lengths are about 3.0 and 4.0 μs, respectively, for the 2.5 mm and 4.0 mm probe in each BABA pulse block. The $^{29}Si$ 90° pulse length was 13 μs, and a recycle delay of 5 s was used. The magnetization of $^{31}P$ of P, P-[3] ferrocenophanes was obtained by preceding the DRENAR sequence by a $^{31}P\{^1H\}$ cross polarization (CP) step. The 90° pulse lengths of $^1H$ and $^{31}P$ are 4.25 μs and 4.0 μs, respectively. The power level on the $^1H$ channel during the contact time was linearly ramped, corresponding to nutation frequencies ranging from 58.8 kHz to 29.4 kHz. The $^{31}P$ nutation frequency was held constant at 42.0 kHz. A contact time of 2 ms was used. All the CSA values used in Table 1 are from the references indicated above except those for $Ag_7P_3S_{11}$ and $CdPS_3$, which are taken from Ref. [33].

## Acknowledgments

This work was supported by the Deutsche Forschungsgemeinschaft through the programme SFB858, the National Natural Science Foundation of China with the Grant number NSFC 61475174, the 100 Talents Program of Chinese Academy of Sciences and Open Fund from State Key Laboratory of Silicate Materials for Architectures (Wuhan University of Technology). HE also acknowledges support by FAPESP, Grant number 2013/07793-6 (CERTEV – *Center for Research, Technology and Education in Vitreous Materials*). We thank the following colleagues for providing samples that had been previously studied collaboratively: Prof. Dr. Gerhard Erker (Organisch-Chemisches Institut, WWU Münster) for three P,P-ferrocenophane samples and Prof. Rainer Pöttgen (Institut für Anorganische und Analytische Chemie, WWU Münster) for a sample of $^{29}Si$-enriched $Li_{13}Si_4$.

## Appendix A. Supplementary material

Supplementary data associated with this article can be found in the online version at http://dx.doi.org/10.1016/j.ssnmr.2015.10.007.

## References

[1] (a) A. Abragam, The Principles of Nuclear Magnetism, Oxford university press, Oxford (1961), p. 103;
(b) C.P. Slichter, Principles of Magnetic ResonanceSpringer Verlag, Heidelberg (1978), p. 371.
[2] M. Duer, Introduction into Solid State NMR Spectroscopy, (Blackwell Publishing Ltd., Oxford (2004), p. 151.
[3] K. Schmidt-Rohr, H.W. Spiess, Multidimensional Solid-State NMR and Polymers, Academic Press, London (1994), p. 402.
[4] G. Brunklaus, H.W. Spiess, H. Eckert, in Modern Methods in Physical Chemistry, First Edition. R. Schäfer, P.C. Schmidt, eds., Wiley-VCH Verlag GmbH & Co., Weinheim, 2012, p. 87–158 and references therein.
[5] T. Gullion, J. Schaefer, J. Magn. Reson. 81 (1989) 196–200.
[6] M. Emshwiller, E.L. Hahn, D. Kaplan, Phys. Rev. 118 (1960) 414.
[7] M. Engelsberg, R.E. Norberg, Phys. Rev. B 5 (1972) 3395.
[8] D. Lathrop, D. Franke, R. Maxwell, T. Tepe, R. Flesher, Z. Zhang, H. Eckert, Solid State Nucl. Magn. Reson. 1 (1992) 73.
[9] D. Lathrop, H. Eckert, J. Am. Chem. Soc. 111 (1989) 3536.
[10] D.E. Kaplan, E.L. Hahn, J. Phys. Radium 19 (1958) 821.
[11] D.M. Gregory, M.A. Mehta, J.C. Shiels, G.P. Drobny, J. Chem. Phys. 107 (1997) 28.
[12] A.E. Bennett, J.H. Ok, R.G. Griffin, S. Vega, J. Chem. Phys., 96, (1992) 8624.
[13] J. Leppert, O. Ohlenschläger, M. Görlach, R. Ramachandran, J. Biomol. NMR 28 (2004) 229.
[14] M.L. Gilchrist Jr., K. Monde, Y. Tomita, T. Iwashita, K. Nakanishi, A. E. McDermott, J. Magn. Reson. 152 (2001) 1.
[15] K. Hu, R. Tycko, J. Chem. Phys. 131 (2009) 45101.
[16] G. De Paepe, Ann. Rev. Phys. Chem 63 (2012) 661.
[17] M. Bjerring, N. Khaneja, N.C. Nielsen, J. Chem. Phys. 130 (2009) 225103.
[18] N. Khaneja, N.C. Nielsen, J. Chem. Phys. 128 (2008) 15103.
[19] B. Hu, L. Delevoye, O. Lafon, J. Trébosc, J.P. Amoureux, J. Magn. Reson. 200 (2009) 178.
[20] A.E. Bennett, D.P. Weliky, R. Tycko, J. Am. Chem. Soc. 120 (1998) 4897.
[21] Y. Ishii, J. Chem. Phys. 114 (2001) 8473.
[22] M. Hohwy, H.J. Jakobsen, M. Edén, M.H. Levitt, N.C. Nielsen, J. Chem. Phys. 108 (1998) 2686.
[23] W. Sommer, J. Gottwald, D.E. Demco, H.W. Spiess, J. Magn. Reson. A 112 (1995) 131.
[24] M. Carravetta, M. Edén b, X. Zhao, A. Brinkmann, M.H. Levitt, Chem. Phys. Lett. 321 (2000) 205.
[25] C.M. Rienstra, M.E. Hatcher, L.J. Mueller, B. Sun, S.W. Fesik, R.G. Griffin, J. Am. Chem. Soc. 120 (1998) 10602.
[26] G. Pileio, M. Concistrè, N. McLean, A. Gansmüller, R.C.D. Brown, M.H. Levitt, J. Magn. Reson. 186 (2007) 65.
[27] S. Olejniczak, P. Napora, J. Gajda, W. Ciesielski, M.J. Potrzebowski, Solid State Nucl. Magn. Reson. 30 (2006) 141.
[28] (a) J. Schmedt auf der Günne, H. Eckert, Chem. Eur. J. 4 (1998) 1762;
(b) J. Schmedt auf der Günne, J. Magn. Reson. 165 (2003) 18.
[29] Y. Tseng, Y. Mou, C. Mou, J.C.C. Chan, Solid State Nucl. Magn.Reson. 27 (2005) 266.
[30] M. Baldus, B.H. Meier, J. Magn. Reson. 128 (1997) 172.
[31] a) K. Saalwächter, F. Lange, K. Matyjaszewski, C.-F. Huang, R.J. Graf, J. Magn. Reson 212 (2011) 204;
b) K. Saalwächter, P. Ziegler, O. Spyckerelle, B. Haidar, A. Vidal, J.U. Sommer, J. Chem. Phys 119 (2003) 3468.
[32] J. Ren, H. Eckert, Angew. Chem. Int. Ed. 51 (2012) 12888.
[33] J. Ren, H. Eckert, J. Chem. Phys. 138 (2013) 164201.
[34] K. Saalwächter, J. Chem. Phys. 141 (2015) 064201.
[35] M. Feike, D.E. Demco, R. Graf, J. Gottwald, S. Hafner, H.W. Spiess, J. Magn. Reson. A 122 (1996) 214.
[36] M. Bak, J.T. Rasmussen, N.C. Nielsen, J. Magn. Reson. 147 (2000) 296.
[37] C. Brinkmann, H. Eckert, D. Wilmer, M. Vogel, J. Schmedt auf der Guenne, W. Hoffbauer, F. Rau, A. Pfitzner, Solid State Sci. 6 (2004) 1077.
[38] F. Boucher, M. Evain, R. Brec, J. Alloy. Compd. 215 (1994) 63.
[39] C.A. Fyfe, H. Meyer zu Altenschildesche, J. Skibsted Inorg. Chem. 38 (1999) 84.
[40] T. Wiegand, H. Eckert, J. Ren, G. Brunklaus, R. Fröhlich, C.G. Daniliuc, G. Lübbe, K. Bussmann, G. Kehr, G. Erker, S. Grimme, J. Phys. Chem. A 118 (2014) 2316.
[41] S. Dupke, T. Langer, R. Pöttgen, M. Winter, S. Passerinia, H. Eckert, Phys. Chem. Chem. Phys. 14 (2012) 6496.